Synthesis, Characterization and Magnetotransport Behavior of La-Based Double Layered Manganites

Y.S. Reddy*

Department of Physics, Chaitanya Bharathi Institute of Technology (A), Hyderabad 500 075, Telangana State, India

(Received December 4, 2016; revised version May 15, 2017; in final form May 18, 2017)

The single phase double layered manganites $La_{1.2}Sr_{1.8-x}Ca_xMn_2O_7$ ($x = 0.0$, 0.3) were synthesized by the sol-gel method. The electrical resistivity at various magnetic fields over a temperature range 4.2–300 K was measured. The insulator-to-metal transition temperature (T_{IM}) decreases from 123 K ($x = 0.0$) to 70 K ($x = 0.3$). The spin-glass (SG)-like transition is observed in both the samples at 30 K (T_{SG} — SG-like transition temperature). The transport behavior is analyzed in the entire temperature range (4.2–300 K) in three different regions: paramagnetic insulating region ($T > T_{IM}$), ferromagnetic metallic region ($T_{SG} < T < T_{IM}$) and antiferromagnetic insulating region ($T < T_{SG}$) by fitting the equations governing the conduction process to the temperature dependent resistivity data in different temperature regions. The results indicate that the Mott variable range hopping (VRH) dominates the transport behavior at $T > T_{IM}$ in the two samples. At $T_{SG} < T < T_{IM}$, the conduction follows the Zener polynomial law $\rho = \rho_0 + \rho_2 T^2 + \rho_{4.5} T^{4.5}$ which suggests the contribution of two-magnon scattering process to the conduction. The zero field conductivity at $T < T_{SG}$ obeys $T^{1/2}$ dependence, consistent with weak localization effects.

DOI: 10.12693/APhysPolA.131.1544

PACS/topics: double layered manganites, electrical transport, magnetoresistance, variable range hopping, spin-glass-like behavior, magnon scattering

1. Introduction

The discovery of colossal magnetoresistance (CMR) in quasi two-dimensional (2D) double layered (DL) manganites $La_{2-2x}Sr_{1+2x}Mn_2O_7$ (LSMO) has drawn much attention due to its reduced dimensionality and structural anisotropy which result in anisotropic characteristics in charge transport and magnetic properties [1–5]. This property of exhibiting CMR effect over a wide temperature region supplies the potential applications for DL manganites. The DL perovskites compound $La_{2-2x}A_{1+2x}Mn_2O_7$ (A is a divalent alkaline earth element) consists of the MnO_2 bilayers and rock-salt-type $(La,A)_2O_2$ layers. The MnO_2 bilayers are separated by rock-salt-type $(La,Sr)_2O_2$ layers along the c-axis [6]. It is found that the magnetic coupling between Mn t_{2g} local spins in the MnO_2 bilayers is at least an order of magnitude stronger than that of inter-bilayers. In addition, the layered manganites provide new interesting physics due to its quasi 2D character, such as enhanced fluctuation effects in the sense of reducing the insulator-to-metal transition (IMT) temperature and correspondingly enhanced magnetoresistance (MR) [7]. The two important interactions between Mn ions, namely double exchange (DE)-driven ferromagnetic (FM) interactions and superexchange (SE)-driven antiferromagnetic (AFM) interactions, are responsible for the observed transport and magnetic properties of the manganites. In the DE mechanism, there will be simultaneous transfer or hopping of an itinerant e_g electron from an Mn^{3+} ion to the nearby O^{2-} ion and from an O^{2-} ion to the neighboring Mn^{4+} ion. When the electron reaches Mn^{4+}, its spin will be the same as that of the electron which left the Mn^{4+} ion. The DE type of e_g electron transfer results in a FM ground state that is conducting. In the SE mechanism, the spin coupling takes place between either Mn^{3+} and Mn^{3+} or Mn^{4+} ions and Mn^{4+} ions through O^{2-} ions, without charge transfer. The SE interaction results in an AFM ground state that is insulating. Because of the reduced dimensionality, the balance between FM-DE and AFM-SE interactions between Mn ions is more subtle and is expected to be responsible for unusual transport properties observed in the DL manganites [8, 9]. Therefore, one can expect that the slight changes in the size and/or concentration of (La,A) site ions can show significant effect on bulk transport and magnetic properties. Further, the Mn–O–Mn bond angle is about 180° in the $(La,A)_3Mn_2O_7$ system and is about 155–170° in $(La,A)MnO_3$ system. The bond-length can be altered by the internal pressure, i.e., by changing the size and/or concentration of (La,A) site ions, however, the variation of the Mn–O–Mn bond-length in Mn_2O_7 system is different from that in MnO_3 system [10–12]. Therefore, the study of lattice effects on the magnetotransport properties in the $(La,A)_3Mn_2O_7$ system might be useful in understanding the fundamentals of the CMR and its related properties.

As the DL manganite system $(La,A)_3Mn_2O_7$ shows various transitions with temperature, the temperature dependent resistivity data of DL manganites should be analyzed in three different temperature regions, namely paramagnetic insulating region ($T > T_{IM}$), ferromagnetic metallic region ($T_{SG} < T < T_{IM}$) and

*e-mail: ysreddy.ou@gmail.com

low temperature upturn region ($T < T_{SG}$). Although, some good number of attempts have been made to explore the nature of conduction mechanism of these layered mangnaites at $T > T_{IM}$ [13–20], the transport behavior at $T_{SG} < T < T_{IM}$ and $T < T_{SG}$ is still unclear. In this paper, the conduction mechanism of $La_{1.2}Sr_{1.8-x}Ca_xMn_2O_7$ ($x = 0.0$, 0.3) is explained in the temperature range 4.2–300 K considering different temperature regions.

Some crystalline and electrical results of $La_{1.2}Sr_{1.8-x}Ca_xMn_2O_7$ (LSCMO)($x = 0.0$, 0.3) were reported by the authors [16], but this article is mainly focused on the conduction mechanism in the temperature range 4.2–300 K. The samples were formed in single phase with body-centered tetragonal structure. The insulator-to-metal transition temperature is 123 K for LSMO and 70 K for LSCMO. Further, the two samples exhibit spin-glass (SG)-like transition at 30 K (T_{SG}). The reason for increasing resistivity with Ca^{2+} doping and the origin of SG-like behavior was also discussed. Further, LSCMO exhibits MR of $\approx 91\%$ at T_{IM} and shows $\approx 30\%$ of MR at 70 K with $H = 0.5$ T, which is indeed a sign of low field magnetoresistance.

2. Experiment

Polycrystalline bulk samples of $La_{1.2}Sr_{1.8-x}Ca_xMn_2O_7$ ($x = 0.0$, 0.3) were prepared by the sol-gel method [16, 21]. High pure powders of La_2O_3, $MnCO_3$, $Sr(NO_3)_2$ and $Ca(NO_3)_2{\cdot}4H_2O$, in stoichiometric proportions, were used. La_2O_3 and $MnCO_3$ were converted into nitrates prior to use. All the nitrates were dissolved in the citric acid solution and then the pH was adjusted to 6 with ammonia solution. After getting the water evaporated, ethylene glycol was added and heated at about 90 °C until a gel-type solution is formed. The gel was dried at 150 °C and then decomposed at 250 °C in air for 2 h to decompose the nitrates and all organic materials. The resultant ash was ground to obtain a fine homogeneous powder. The powder was calcinated in air at 1100 °C for 10 h and then pressed into circular pellets. The pellets were finally sintered in air at 1400 °C for 6 h. The structural characterization was carried out by powder X-ray diffraction using Xpert pro system, M/s PANalytical ($\lambda = 1.54056$ Å) in 2θ range 20°–80°, with step size 0.01° and a count time of 0.6 s per step. The zero field and field dependent ($H = 1.5$ T, 4 T) electrical resistivity measurements were carried out by standard four-probe method over the temperature range 4.2–300 K with the use of a superconducting magnet system of OXFORD.

3. Results and discussion

3.1. Electrical transport

To find the nature of the transport behavior, the $\rho{-}T$ data in the entire temperature range (4.2–300 K) are analyzed in three different temperature regions: (i) paramagnetic insulating region ($T > T_{IM}$), (ii) ferromagnetic metallic region ($T_{SG} < T < T_{IM}$) and (iii) antiferromagnetic insulating region ($T < T_{SG}$).

3.1.1. Paramagnetic insulating region ($T > T_{IM}$)

Generally, electron hopping is of variable range type at low temperatures, where the thermal energy is not great enough to allow electrons to hop to their nearest neighbors. In that case, electrons choose to hop further to find a smaller potential difference. At high temperatures, conduction may be by activation by mobility edge or narrow band gap. In the intermediate temperature range, nearest neighbor (small polaron) hopping dominates [22].

The conduction mechanism in PM semiconducting/insulating region in manganites is usually explained by four models. They are: (i) semiconduction (SC) model described by the Arrhenius equation $\rho = \rho_0 \exp(E_a/k_BT)$ [23], (ii) nearest neighbor small polaron hopping (SPH) model described by $\rho = \rho_0 T^n \exp(E_p/k_BT)$, where $n = 1$ for adiabatic hopping [24] and $n = 1.5$ for non-adiabatic hopping [25], (iii) the Mott type of variable range hopping (VRH) model described by $\rho = \rho_\infty \exp(T_0/T)^p$, where $p = 1/(d+1)$, d being the dimensionality of the system [26, 27] and (iv) the Efros–Shklovskii (ES) type of VRH model described by $\rho = \rho_\infty \exp(T_0/T)^{1/2}$ [27, 28]. Here, ρ_0 is a pre-factor in SC and SPH models and ρ_∞ is a pre-factor in VRH models. E_a and E_p are the activation energies in SC model and SPH model, respectively. T_0 is characteristic temperature in VRH models and its value in the Mott VRH model is given by $24/\pi L^d k_B N(E_F)$, where L is localization length of trapped charge carriers (here $L = 10^{-10}$ m), $N(E_F)$ is density of the localized states at the Fermi level and d is the dimensionality of the system. The Coulomb interaction in hopping regime which produces a gap in electronic density of states (DOS) is responsible for ES VRH type of conduction mechanism, whereas the Mott VRH arises when such gap is filled. Each predicts a different temperature dependence of the resistivity and fits the resistivity data in different temperature ranges.

In case of cubic perovskite manganites, the conduction above T_{IM} generally obeys either the Mott 3D VRH or SPH model [26, 28, 29]. But, the DL manganites, because of their quasi-2D nature, are expected to exhibit some complexity in their transport behavior. Here, the presence of the Coulomb gap and the dimensionality of the materials are to be considered in order to evaluate the nature of conduction mechanism. In case of DL manganites, the conduction at $T > T_{IM}$ is explained by Matsukawa et al. [13], Hong Zhu et al. [14], and others [15, 16] using the Mott type VRH while Chatterjee et al. [10], Ang et al. [17], and others [18, 19] suggested SPH model. Chen et al. [20] suggested ES VRH type of conduction in similar DL manganites.

In the present study, the $\rho{-}T$ data are analyzed by fitting all the equations mentioned above to $\rho{-}T$ data.

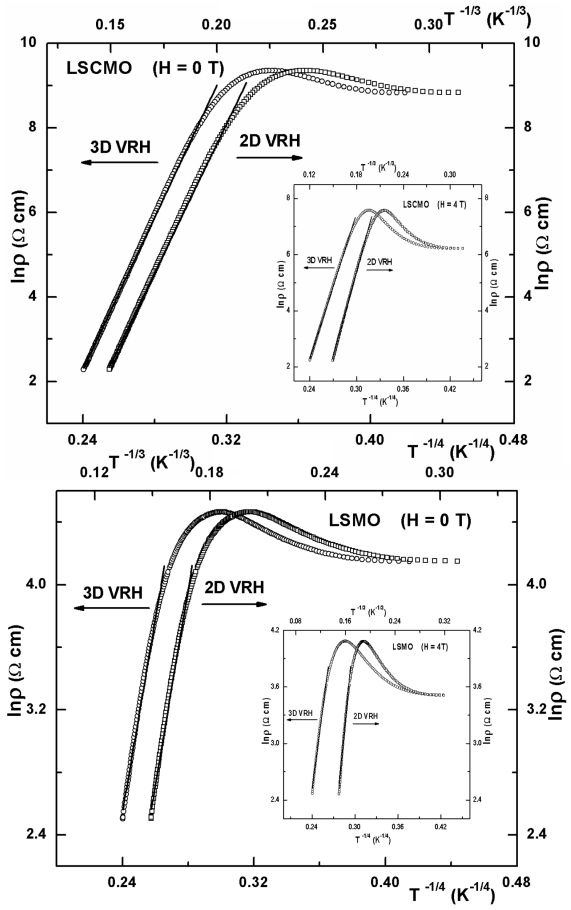

Fig. 1. Plots of lnρ vs. $T^{-1/4}$ and lnρ vs. $T^{-1/3}$ for LSMO and LSCMO. The solid lines give the best fits to the Mott 2D and 3D VRH models.

The equations of SC and SPH models do not fit well to ρ–T data for the two samples; ES VRH gives reasonably good fittings for LSCMO sample only and the best fittings, for the two samples, are obtained with the Mott VRH model over a wide temperature range (Fig. 1). The Mott 2D and 3D VRH models give almost indistinguishable fittings for drawing any conclusion about dimensionality dependence, the results clearly point towards the Mott type of VRH conduction mechanism in paramagnetic insulating region ($T > T_{IM}$). The reason for obtaining reasonably good fittings for LSCMO sample with ES VRH model may be due to its high resistivity where the electron–electron Coulomb interactions are present. The best fit parameters obtained with the Mott 2D and 3D VRH models are listed in Table I and they are in good agreement with the previous reports on similar DL manganites [13–16, 30]. The goodness of the fit is indicated by the value of R^2. The values of R^2 are close to unity and suggest the reliability of the fittings.

Further, the variation of T_{IM} and ρ_{IM} with Ca^{2+} doping can be explained in terms of characteristic temperature (T_0), obtained from the fitting of resistivity data to the Mott VRH model. Since T_0 is inversely related to the extent of the localized states, the increasing value of

TABLE I

The best-fit parameters obtained from the Mott VRH model fittings for LSMO and LSCMO.

Sample	H [T]	T_{rg} [K]	T_0 [K]	ρ_∞ [Ωcm]	$N(E_F)$ [$\frac{1}{\text{eV cm}^4}$]	R^2
Mott 3D VRH						
LSMO	0	>200	1.44×10^7	4.77×10^{-6}	6.13×10^{21}	0.9911
	4	>210	1.12×10^7	11.44×10^{-6}	7.90×10^{21}	0.9917
LSCMO	0	>100	6.62×10^7	3.91×10^{-9}	1.34×10^{21}	0.9984
	4	>125	5.60×10^7	9.32×10^{-9}	1.58×10^{21}	0.9986
Mott 2D VRH						
LSMO	0	>200	3.92×10^5	2.31×10^{-4}	2.26×10^{15}	0.9902
	4	>210	3.26×10^5	4.32×10^{-4}	2.72×10^{15}	0.9909
LSCMO	0	>100	1.13×10^6	1.84×10^{-6}	7.85×10^{14}	0.9975
	4	>125	1.02×10^6	2.97×10^{-6}	8.66×10^{14}	0.9970

T_0 shows that with increase of Ca^{2+} content, the localization length and hence the hopping distance decreases. The conjecture regarding the localization length and hopping distance suggests that with an increase of Ca^{2+} content, i.e., increased distortion of the MnO_6 octahedron, the hole mobility decreases, and hence ρ_{IM} increases and T_{IM} decreases. The pre-factor ρ_∞ is known as the high temperature limit of resistivity in the Mott VRH model and its variation with Ca^{2+} content is in accordance with the variation of resistivity at 300 K with Ca^{2+} content. The decreasing value of $N(E_F)$ from LSMO to LSCMO also indicates that the ability to conduct decreases from LSMO to LSCMO. The decreasing value of T_0 and increasing value of $N(E_F)$ for a given sample with the application of magnetic field is due to the suppression of magnetic domain scattering with the application of magnetic field [29].

3.1.2. Ferromagnetic metallic region ($T_{SG} < T < T_{IM}$)

The temperature dependent resistivity of cubic perovskite rare-earth manganites in FM metallic region ($T < T_{IM}$) has been studied by many researchers, by fitting the general Zener DE polynomial law $\rho = \rho_0 + \rho_2 T^2 + \rho_n T^n$ to ρ–T data [24, 28, 29, 31–33]. Here, ρ_0 is the residual resistivity and is independent of temperature, ρ_2 is the resistivity contributed by electron–electron and electron–phonon scattering mechanisms and ρ_n is the resistivity coefficient corresponding to n, which takes values from 2.5 to 7.5. However, the most preferred values for n are 2.5, 4.5, and 7.5. The value of n is included by taking spin fluctuations into account. Further, the low value of n (< 4.5) corresponds to one-magnon scattering process, whereas the high value of n (≥ 4.5) corresponds to two-magnon scattering process. Apart from this, some explained the transport behavior using $\rho = \rho_0 + \rho_2 T^2$ [24, 34], without including the magnon contribution and some other explained the transport behavior using $\rho = \rho_0 + \rho_{2.5} T^{2.5}$ [29, 35], where the conduction is dominated by one-magnon scattering alone.

The transport behavior at $T < T_{IM}$ in polycrystalline DL manganites has not been studied much unlike the transport mechanism at $T > T_{IM}$ in layered manganites

and one can find a very few reports in the literature. The reason may be due to the absence of T_{IM} in many DL manganites and a small temperature range between T_{IM} and T_{SG}. Zhang et al. [9] found $T^{9/2}$ dependence in single crystals of $La_{1.2}Sr_{1.8}Mn_2O_7$, but they did not include $\rho_2 T^2$ term. Therefore, to find the suitable law governing the variation of resistivity at $T_{SG} < T < T_{IM}$, we fitted the $\rho-T$ data of the two samples to the polynomial law, taking the value of n from 2.5 to 7.5 and also to the equations $\rho = \rho_0 + \rho_2 T^2$ and $\rho = \rho_0 + \rho_{2.5} T^{2.5}$.

The Zener polynomial law with $n = 4.5$ fits well to $\rho-T$ data of the two samples (both in absence and in presence) in the wide temperature range (Fig. 2 and Table II) and suggests the two-magnon scattering process in this temperature range along with electron–electron and electron–phonon scattering mechanisms. When magnetic field is applied, the fitting range increases as T_{IM} shifts to higher temperature and the best fit parameters ρ_0, ρ_2 and $\rho_{4.5}$ (for $n = 4.5$) show a decreasing trend with the applied magnetic field. The applied magnetic field can decrease the magnetic domain boundary and therefore ρ_0 decreases. The magnetic field can suppress the electron–electron scattering and spin fluctuations and hence ρ_2 and $\rho_{4.5}$ decrease with magnetic field [28, 29]. All the fitting parameters, i.e., ρ_0, ρ_2 and $\rho_{4.5}$ of LSCMO are much greater than those of LSMO and this indicates the mechanisms contributing to ρ_0, ρ_2 and $\rho_{4.5}$ terms become strong in LSCMO. Particularly, the value of the term $\rho_{4.5}$, which arises from spin fluctuations, is much higher for LSCMO than that for LSMO indicating the pronounced spin fluctuations in this LSCMO sample, which reflects in its high resistivity. The values of R^2 are also listed in Table II.

TABLE II

The best-fit parameters obtained from fitting $\rho = \rho_0 + \rho_2 T^2 + \rho_{4.5} T^{4.5}$ to $\rho-T$ data.

Sample	Fitting region	ρ_0 [Ωcm]	ρ_2 [Ωcm/K^2]	$\rho_{4.5}$ [Ωcm/K$^{4.5}$]	R^2
$H = 0$ T					
TLSMO	30–100 K	60.1	0.0021	1.36×10^{-9}	0.9964
LSCMO	30–60 K	5893.3	0.5715	2.81×10^{-5}	0.9946
$H = 4$ T					
LSMO	0–120 K	31.2	0.0016	0.65×10^{-9}	0.9972
LSCMO	0–90 K	423.6	0.0462	0.17×10^{-5}	0.9953

Interestingly, when we tried to fit the polynomial law by taking $n = 5.5$, 6.5, and 7.5 to $\rho-T$ data, we obtained reasonably good fittings in the absence of magnetic field (Fig. 3). This may indicate the possibility of higher order magnon scattering in these samples in the absence of magnetic field which shifts to lower order electro-magnon scattering under the magnetic field of 4 T [28]. When magnetic field of 4 T is applied, the spin fluctuations are suppressed and as a result higher magnon scattering term becomes negligible and hence the resistivity data cannot be fitted to the polynomial law with $n > 4.5$.

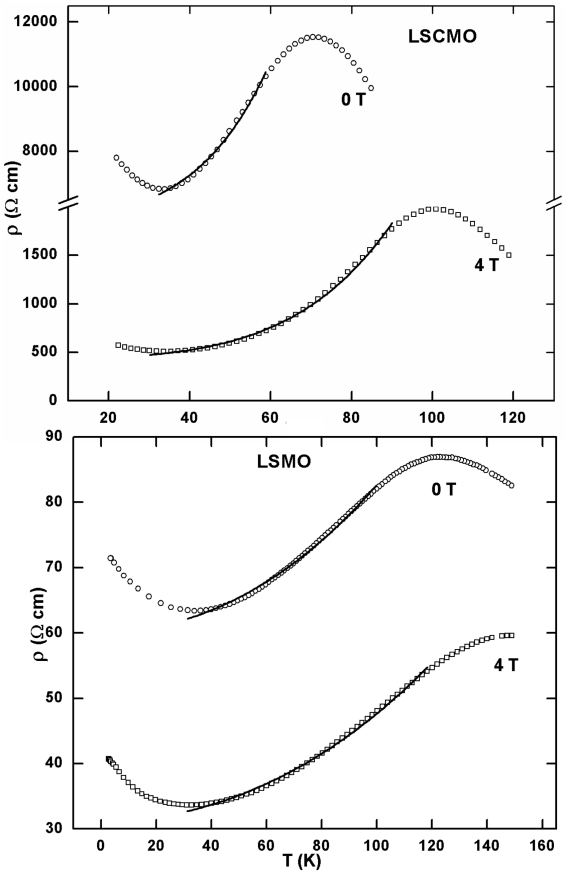

Fig. 2. ρ vs. T plots for LSMO and LSCMO. The solid lines give the best fits to the equation $\rho = \rho_0 + \rho_2 T^2 + \rho_{4.5} T^{4.5}$.

3.1.3. Antiferromagnetic insulating region ($T < T_{SG}$)

The low temperature upturn of resistivity is a typical characteristic of DL manganites. The transport behavior of DL manganites in AFM insulating region ($T < T_{SG}$) is very interesting and worthy of study. Earlier, Zhu et al. [14] found the band transport process at $T < T_{SG}$ in polycrystalline $La_{1.4}Sr_{1.6}Mn_2O_7$, Zhang et al. [36] fitted the upturn of resistivity using the Mott VRH equation in polycrystalline Co doped $LaSr_2Mn_2O_7$ and Zhang et al. [9] and Okuda et al. [37] showed that conductivity σ is proportional to $T^{1/2}$ in single crystals of DL manganites. The $T^{1/2}$ dependence of conductivity is a characteristic of weak localization effects in 3D disordered metals and indicate the contribution of electron–electron interactions to the conductivity.

To find the nature of the transport mechanism at $T < T_{SG}$ in the present DL manganite samples, the four equations mentioned in Sect. 3.1.1 are fitted to $\sigma-T$ data at $T < T_{SG}$ and $T^{1/2}$ dependence of σ is also examined. When no magnetic field is applied, the conductivity of the two samples obeys $T^{1/2}$ dependence (fitting range: 4.2–30 K) while all the other conduction models fail to give good fittings (Fig. 4). The $T^{1/2}$ dependence of σ ($H = 0$ T) indicates the contribution of electron–electron

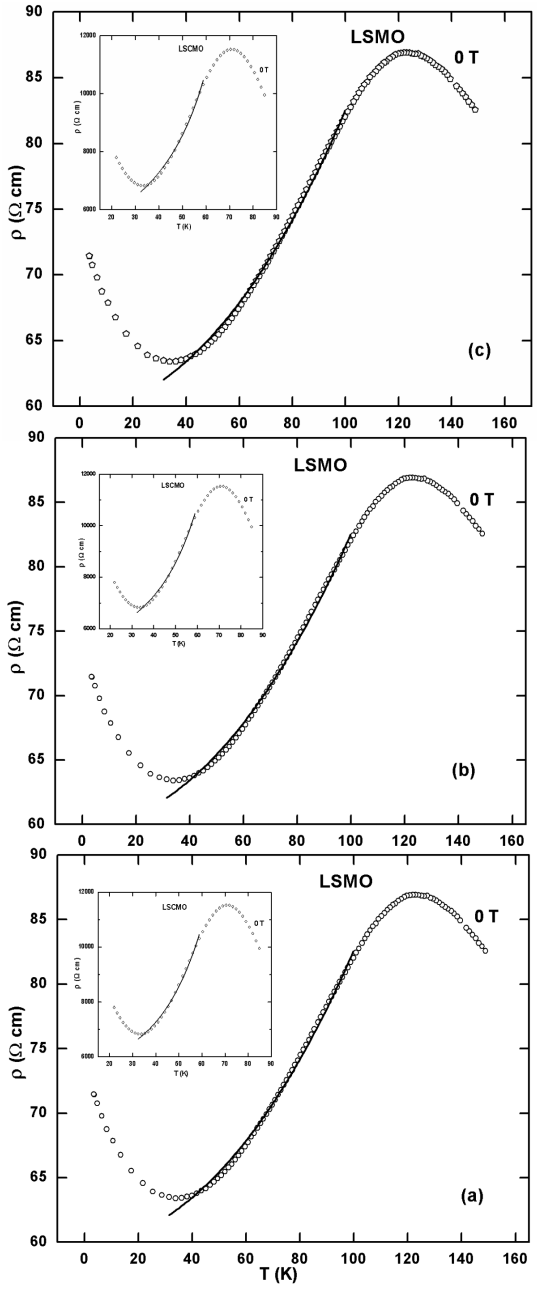

Fig. 3. ρ vs. T plots for LSMO and LSCMO. The solid lines give the best fits to the equations $\rho = \rho_0 + \rho_2 T^2 + \rho_{5.5} T^{5.5}$ (a), $\rho = \rho_0 + \rho_2 T^2 + \rho_{6.5} T^{6.5}$ (b), and $\rho = \rho_0 + \rho_2 T^2 + \rho_{7.5} T^{7.5}$ (c).

interactions to the conductivity at very low temperature and is consistent with 3D weak localization effects in disordered metals [9, 37].

In the presence of magnetic field of 4 T, LSMO and LSCMO samples give the best fittings with VRH models (fitting range 4.2–30 K) which may suggest that VRH process is initiated under the presence of magnetic field of 4 T. It is observed that the Mott VRH model is suitable for LSMO; nevertheless, it is difficult to conclude about dimensionality dependence as both the Mott 2D and 3D VRH models give almost indistinguishable fittings. For LSCMO, the temperature dependent conductivity σ ($H = 4$ T) follows ES VRH law, which may be attributed to its high resistivity where the electron–electron Coulomb interactions contribute significantly to the conduction. The crossover from the high temperature Mott VRH mechanism to low temperature ES VRH mechanism is observed as temperature recedes from high to low because at higher temperature hopping becomes much larger than the Coulomb gap and its effect is suppressed [38]. The obtained results clearly indicate that electron–electron interactions are present in the entire temperature range (4.2–300 K) in LSCMO.

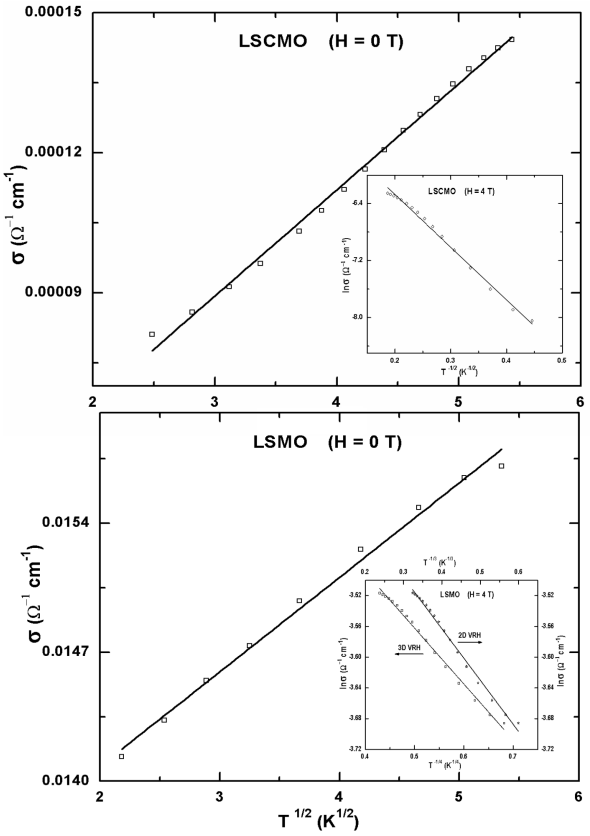

Fig. 4. σ ($H = 0$ T) vs. $T^{1/2}$ plots for LSMO and LSCMO. The solid lines give the best fits of the data with a $T^{1/2}$ dependence. Insets: plots of $\ln\sigma$ vs. $T^{-1/4}$ and $\ln\sigma$ vs. $T^{-1/3}$ for LSMO and $\ln\sigma$ vs. $T^{-1/2}$ for LSCMO ($H = 4$ T). The solid lines give the best fits to the Mott 2D and 3D VRH models (LSMO) and ES VRH model (LSCMO).

4. Conclusion

DL manganite samples $La_{1.2}Sr_{1.8-x}Ca_xMn_2O_7$ ($x = 0.0, 0.3$) were prepared by the sol–gel method and their magnetotransport properties were investigated in the temperature range 4.2–300 K. The T_{IM} is found to decrease with Ca^{2+} doping and the two samples show SG-like

behavior below 30 K. In the two samples, the conduction process at $T > T_{IM}$ is due to the Mott VRH mechanism. At $T_{SG} < T < T_{IM}$, electron–electron scattering and two-magnon scattering processes contribute to conduction. The zero field conductivity obey $T^{1/2}$ dependence at $T < T_{SG}$, which is consistent with weak localization effects in 3D disordered metals and the conductivity in the presence of magnetic field follow VRH process in the two samples. The electron–electron interactions are seen in LSCMO sample at the entire temperature range 4.2–300 K.

References

[1] Y. Moritomo, A. Asamitsu, H. Kuwahara, Y. Tokura, *Nature (London)* **380**, 141 (1996).

[2] T. Kimura, Y. Tomioka, H. Kuwahara, A. Asamitsu, M. Tamura, Y. Tokura, *Science* **274**, 1698 (1996).

[3] T. Kimura, A. Asamitsu, Y. Tomioka, Y. Tokura, *Phys. Rev. Lett.* **79**, 3720 (1997).

[4] D.N. Argyriou, J.F. Mitchell, J.B. Goodenough, O. Chmaissem, S. Short, J.D. Jorgensen, *Phys. Rev. Lett.* **78**, 1568 (1997).

[5] J.F. Mitchell, C.D. Ling, J.E. Millburn, D.N. Argyriou, A. Berger, M. Medarde, *J. Appl. Phys.* **89**, 6618 (2001).

[6] S.N. Ruddlesden, P. Popper, *Acta Crystallogr.* **11**, 54 (1958).

[7] Hong Zhu, Xianming Liu, Keqing Ruan, Yuheng Zhang, *Phys. Rev. B* **65**, 104424 (2002).

[8] S. Okamoto, S. Ishihara, S. Maekawa, *Phys. Rev. B* **63**, 104401 (2001).

[9] C.L. Zhang, X.J. Chen, C.C. Almasan, J.S. Gardner, J.L. Sarrao, *Phys. Rev. B* **65**, 134439 (2002).

[10] S. Chatterjee, P.H. Chou, C.F. Chang, I.P. Hong, H.D. Yang, *Phys. Rev. B* **61**, 6106 (2000).

[11] H. Zhu, D. Zhu, Y. Zhang, *J. Appl. Phys.* **92**, 7355 (2002).

[12] A. Szytula, *Acta Phys. Pol. A* **118**, 303 (2010).

[13] M. Matsukawa, M. Chiba, E. Kikuchi, R. Suryanarayanan, M. Apostu, S. Nimori, K. Sugimoto, N. Kobayashi, *Phys. Rev. B* **72**, 224422 (2005).

[14] Hong Zhu, Xiaojun Xu, Li Pi, Yuheng Zhang, *Phys. Rev. B* **62**, 6754 (2000).

[15] Sunil Nair, A. Banerjee, *Phys. Rev. B* **70**, 104428 (2004).

[16] Y.S. Reddy, V. Prashanth Kumar, R. Rawat, A. Banerjee, P. Kistaiah, C. Vishnuvardhan Reddy, *Phys. Status Solidi B* **244**, 3719 (2007).

[17] R. Ang, W.J. Lu, R.L. Zhang, B.C. Zhao, X.B. Zhu, W.H. Song, Y.P. Sun, *Phys. Rev. B* **72**, 184417 (2005).

[18] X.J. Chen, C.L. Zhang, C.C. Almasan, J.S. Gardner, J.L. Sarrao, *Phys. Rev. B* **67**, 094426 (2003).

[19] R. Thiyagarajan, N. Manivannan, S. Arumugam, S. Esakki Muthu, N.R. Tamilselvan, C. Sekar, H. Yoshino, K. Murata, M.O. Apostu, R. Suryanarayanan, A. Revcolevschi, *J. Phys. Condens. Matter* **24**, 136002 (2012).

[20] X.J. Chen, C.L. Zhang, J.S. Gardner, J.L. Sarrao, C.C. Almasan, *Phys. Rev. B* **68**, 064405 (2003).

[21] Y.S. Reddy, V. Prashanth Kumar, S. Ramesh, S. Venkanna, M.V. Ramana Reddy, P. Kistaiah, C. Vishnuvardhan Reddy, *Acta Phys. Pol. A* **113**, 677 (2007).

[22] M. Viret, L. Ranno, J.M.D. Coey, *Phys. Rev. B* **55**, 8067 (1997).

[23] S.B. Ogale, V. Talyansky, C.H. Chen, R. Ramesh, R.L. Green, T. Venkatesan, *Phys. Rev. Lett.* **77**, 1159 (1996).

[24] G. Jeffrey Snyder, R. Hiskes, S. Dicarolis, M.R. Beasley, T.H. Geballe, *Phys. Rev. B* **53**, 14434 (1996).

[25] M. Jaime, H.T. Hardner, M.B. Salamon, M. Rubinstein, P. Dorsey, D. Emin, *Phys. Rev. Lett.* **78**, 951 (1997).

[26] M. Viret, L. Ranno, J.M.D. Coey, *J. Appl. Phys.* **81**, 4964 (1997).

[27] Yu Wang, J.J. Santiago-Aviles, *Appl. Phys. Lett.* **89**, 123119 (2006).

[28] D.S. Rana, C.M. Thaker, K.R. Mavani, D.G. Kuberkar, D.C. Kundaliya, S.K. Malik, *J. Appl. Phys.* **95**, 4934 (2004).

[29] A. Banerjee, S. Pal, B.K. Chaudhuria, *J. Chem. Phys.* **115**, 1550 (2001).

[30] M.H. Ehsani, P. Kameli, M.E. Ghazi, *J. Phys. Chem. Solids* **73**, 744 (2012).

[31] P. Schiffer, A.P. Ramirez, W. Bao, S.-W. Cheong, *Phys. Rev. Lett.* **75**, 3336 (1995).

[32] M. Ziese, *Rep. Prog. Phys.* **65**, 143 (2002).

[33] Q. Huang, Z.W. Li, J. Li, C.K. Ong, *J. Phys. Condens. Matter* **13**, 4033 (2001).

[34] A. Urushibara, Y. Moritomo, T. Amira, A. Asamitsu, G. Kido, Y. Tokura, *Phys. Rev. B* **51**, 14103 (1995).

[35] Li Pi, Lei Zheng, Yuheng Zhang, *Phys. Rev. B* **61**, 8917 (2000).

[36] R.L. Zhang, W.H. Song, Y.Q. Ma, J. Yang, B.C. Zhao, Z.G. Sheng, J.M. Dai, Y.P. Sun, *Phys. Rev. B* **70**, 224418 (2004).

[37] T. Okuda, T. Kimura, Y. Tokura, *Phys. Rev. B* **60**, 3370 (1999).

[38] I. Shklovskii, A.L. Efros, in: *Electronic Properties of Doped Semiconductors*, Springer- Verlag, Berlin 1984.